DOI: 10.1002/ejic.201000908

# Crystal Structure, Spectroscopy and Crystal Field Analysis of Substituted 1,10-Phenanthroline–Europium Complexes

Zaifa Pan,[a,b] Guohua Jia,[a] Chang-Kui Duan,[a] Wai-Yeung Wong,[c] Wing-Tak Wong,[d] and Peter A. Tanner*[a]

**Keywords:** Luminescence / Electronic structure / Absorbance / Europium

Crystal structures and vibrational and electronic spectroscopic data are reported for europium(III) complexes with 5(or 4)-R-1,10-phenanthroline (phen) ligands (R = chloro, methyl, nitro, amino). All complexes comprise a 10-coordinate $Eu^{3+}$ ion with three chelating nitrato anions and two bidentate phen ligands. The crystal structures are of three distinct types with space groups $C2/c$, $P2_1/n$ and $P\bar{1}$. The room-temperature emission spectra are dominated by the forced electric dipole $^5D_0 \rightarrow {}^7F_2$ emission of $Eu^{3+}$. The excitation spectra show that the triplet donor state of the nitro-substituted complex has a lower energy than the other complexes and the lower luminescence quantum efficiency of this complex is rationalized. The emission spectra recorded at 10 K have been compared with those of the corresponding $Eu^{3+}$-doped yttrium complexes using different excitation lines as a criterion of sample purity. The spectrum of the unsubstituted phen complex is more clearly resolved than those of the other complexes and this has been attributed to disorder resulting in inhomogeneous broadening. A detailed crystal field analysis is given for the phen complex from the fitting of 24 crystal field energy levels. A comparison with other complexes has been made through derived second-rank crystal field strengths. No simple relationships have been derived from comparisons of energy levels, spectral line positions, or second-rank crystal field strengths with crystallographic data or Taft constants.

## Introduction

The design of efficient luminescent organic lanthanide complexes for applications in lighting devices,[1–7] telecommunications,[8,9] nanosensors[10] and bio-imaging[11] has received tremendous attention in recent years. Luminescent lanthanide complexes are of considerable importance due to their unique photophysical properties such as long lifetime (micro- to millisecond) and characteristic and sharp emission bands. Because of the small forced dipole strength of f→f transitions, direct excitation to the 4f excited states of lanthanide complexes is not efficient. An alternative is to employ an organic chromophore as a good light harvester to sensitize lanthanide ions ($Ln^{3+}$) by energy transfer, usually from the triplet state, by the antenna effect.[12–15] The ligand 1,10-phenanthroline (phen) is an excellent antenna with singlet and triplet states at 29200 and 22100 $cm^{-1}$, respectively, and has been employed to sensitize various $Ln^{3+}$ species in crystals and hybrid materials.[16–18] Hasegawa has measured and described the energy transfer from the triplet state of phen to $Ln^{3+} = Pr^{3+}$.[19] In this case, for the complex $[Pr(phen)_2(NO_2)_3]$, the ππ* singlet and triplet states exhibit a redshift and are roughly located (as 0–0 energies) at 27800 and 21560 $cm^{-1}$, respectively.

The structures and luminescence properties of lanthanide nitrates and their derivatives containing phen have previously been investigated.[20–27] The crystal structures of $[Y(phen)_2(NO_3)_3]$ and $[Eu(phen)_2(NO_3)_3]$ were studied by Mirochnik et al.[20] and Boudalis et al.,[21] respectively. Both compounds crystallize in the $C2/c$ space group with the tripositive lanthanide ion situated on a two-fold axis. Puntus and Zolin[25] performed a crystal field calculation for the energy levels of $Eu^{3+}$ in $[Eu(phen)_2(NO_3)_3]$ by assuming the symmetry of the europium polyhedron to be $C_{2v}$. Tsaryuk and co-workers compared the effect of the size of the ligands and their effective charge upon the crystal structures and also upon the vibronic emission spectra of europium nitrates with 1,10-phenanthroline derivatives: 3,4,7,8-tetramethylphenanthroline, 5-methylphenanthroline, 4,7-diphenylphenanthroline and 5-nitrophenanthroline.[22–24] More recently, Puntus and co-workers investigated the structures and luminescence spectra of lanthanide complexes with phen, chloride ions and aqua ligands.[28–30]

In the work reported herein we synthesized the phen and substituted phen complexes $[Eu(NO_3)_3phen_2]$ (**I**), $[Y(NO_3)_3$-

[a] Department of Biology and Chemistry, City University of Hong Kong,
Tat Chee Avenue, Kowloon, Hong Kong S. A. R., P. R. China
E-mail: bhtan@cityu.edu.hk
[b] College of Chemical Engineering and Materials Science, Zhejiang University of Technology,
Hangzhou 310014, Zhejiang, P. R. China
[c] Department of Chemistry, Hong Kong Baptist University,
Waterloo Road, Kowloon Tong, Hong Kong S. A. R., P. R. China
[d] Department of Chemistry, The University of Hong Kong,
Pokfulam, Hong Kong S. A. R., P. R. China
Supporting information for this article is available on the WWW under http://dx.doi.org/10.1002/ejic.201000908.

  

phen$_2$] (**IY**), [Eu(NO$_3$)$_3$(5-nitro-phen)$_2$] (**I-5n**), [Eu(NO$_3$)$_3$(5-methyl-phen)$_2$] (**I-5m**), [Eu(NO$_3$)$_3$(4-methyl-phen)$_2$] (**I-4m**), [Eu(NO$_3$)$_3$(5-amino-phen)$_2$] (**I-5a**) and [Eu(NO$_3$)$_3$(5-chloro-phen)$_2$] (**I-5c**). The analogous complexes were also prepared by doping 0.5 at.-% $Eu^{3+}$ into the corresponding $Y^{3+}$ complexes and these are labelled as **IY(Eu)**, **IY(Eu)-5n**, etc. Our work serves to investigate the crystal structure of europium nitrate complexes containing phen and its derivatives and to evaluate the influence of the steric effects of the substituents of phen on the crystal structure and accordingly the influence of the donor–acceptor properties on the electronic spectra and luminescence quantum efficiency. Crystal field analyses were performed to provide a succinct summary of the electronic properties, which can be compared with physical data.

## Results and Discussion

### Crystal Structures

The crystal structures of **I**, **IY**, **I-5c**, **I-4m** and **I-5m** are displayed in Figure 1 and the crystallographic data are summarized in Table 1. Two independent crystal structure determinations of [Ln(NO$_3$)$_3$(1,10-phen)$_2$] were carried out in 2001 by Boudalis et al.[21] (**IY**) and Mirochnik et al.[20] (**I**) and the results obtained in this work are in agreement, although the latter determination is more accurate. Boudalis et al. pointed out that nitrato complexes of lanthanide ions with metal/phen ratios of 1:1 or 1:3 have not been prepared with the exception of [Yb(NO$_3$)$_3$(1,10-phen)(H$_2$O)]. Detailed crystallographic data for **I** and **IY** from this study are summarized in the Supporting Information together with the data for a diluted crystal of **IY** doped with 0.5% $Eu^{3+}$ (Figures S1–S3, Tables S1–S3). The 10-coordinate geometries of the $Eu^{3+}$ and $Y^{3+}$ ions in **IY** and **I** consist of three *O*,*O*′-bidentate nitrates and two sets of *N*,*N*′ ligands in a spenocorona (tetradecahedron) geometry, which has 14 faces (12 triangles and two squares). The metal ion is situated on a two-fold rotation symmetry axis that passes through one of the N–O bonds of a nitrate anion. In **IY**, the two phen ligands are coplanar with a root mean square deviation of $<0.04$ Å from the mean plane with the $Y^{3+}$ ion $<0.462(2)$ Å above the mean plane. The molecules are

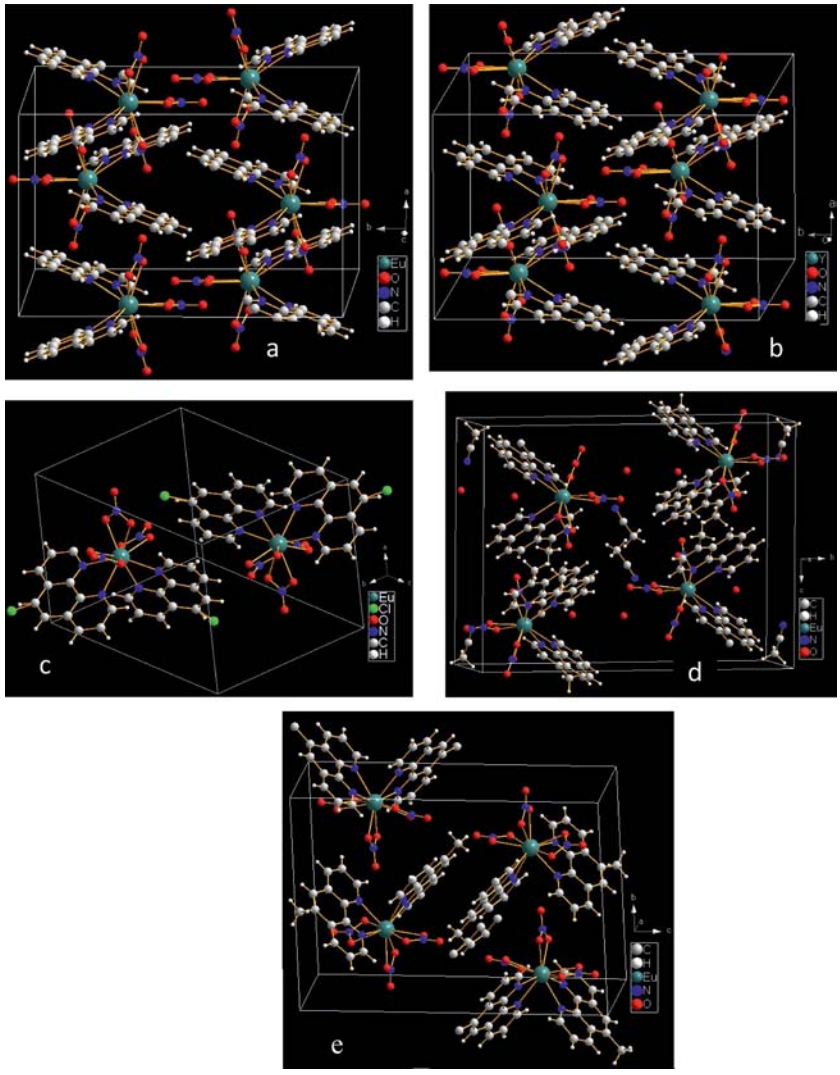


Figure 1. Crystal structures of (a) **I**, (b) **IY**, (c) **I-5c**, (d) **I-4m** and (e) **I-5m**.

  

Table 1. Crystallographic data for [Ln(R-phen)$_2$(NO$_3$)$_3$] complexes [Ln = Eu (**I**), Y (**IY**); R = H (**I**, **IY**), 4-methyl (**I-4m**), 5-methyl (**I-5m**), 5-chloro (**I-5c**)].

| | **I** | **IY** | **I-4m** | **I-5m** | **I-5c** |
|---|---|---|---|---|---|
| Formula | $C_{24}H_{16}N_7O_9Eu$ | $C_{24}H_{16}N_7O_9Y$ | $C_{28}H_{27}N_8O_{11}Eu$ | $C_{26}H_{20}N_7O_9Eu$ | $C_{24}H_{14}Cl_2N_7O_9Eu$ |
| Formula weight | 698.39 | 635.34 | 803.54 | 726.45 | 767.28 |
| Crystal system | monoclinic | monoclinic | monoclinic | monoclinic | triclinic |
| Space group | *C*2/*c* (#15) | *C*2/*c* (#15) | $P2_1/n$ (#14) | $P2_1/c$ (#14) | $P\bar{1}$ (#2) |
| *a* [Å] | 11.1841(15) | 11.1638(13) | 9.888(2) | 9.491(2) | 9.200(2) |
| *b* [Å] | 17.996(2) | 17.891(2) | 22.286(4) | 14.150(2) | 11.273(3) |
| *c* [Å] | 13.0652(18) | 13.021(2) | 17.392(3) | 20.513(3) | 13.803(3) |
| *α* [°] | 90 | 90 | 90 | 90 | 98.082(4) |
| *β* [°] | 100.560(2) | 100.505(2) | 92.310(3) | 96.845(3) | 105.705(4) |
| *γ* [°] | 90 | 90 | 90 | 90 | 99.813(4) |
| *V* [Å$^3$] | 2585.0(6) | 2557.1(5) | 3830(1) | 2735.1(8) | 1331.3(5) |
| *Z* | 4 | 4 | 4 | 4 | 2 |
| $D_{calcd.}$ [g cm$^{-3}$] | 1.794 | 1.650 | 1.394 | 1.764 | 1.914 |
| $\mu$ [mm$^{-1}$] | 2.494 | 2.352 | 1.698 | 2.361 | 2.619 |
| *F*(000) | 1376 | 1280 | 1608 | 1440 | 752 |
| $\theta$ range [°] | 2.24–27.51 | 2.26–27.45 | 2.25–25.00 | 2.46–28.36 | 2.32–27.55 |
| Reflections collected | 8579 | 7686 | 18462 | 16441 | 9036 |
| Unique reflections | 2971 | 2885 | 6628 | 6575 | 5900 |
| $R_{int.}$ | 0.030 | 0.028 | 0.0910 | 0.0680 | 0.047 |
| Observed reflections [$I > 2\sigma(I)$] | 3351 | 2352 | 3351 | 3666 | 4549 |
| Number of parameters | 190 | 196 | 409 | 388 | 421 |
| *R*1, *wR*2 [$I > 2\sigma(I)$][a] | 0.0190, – | 0.025, 0.029 | 0.0716, 0.1731 | 0.0518, 0.1050 | 0.0432, 0.0482 |
| *R*1, *wR*2 (all data) | 0.0205, 0.0541 | | 0.1459, 0.2180 | 0.1145, 0.1271 | |
| GoF on $F^2$[b] | 1.053 | 1.045 | 0.964 | 1.001 | 1.040 |

[a] $R1 = \Sigma||F_o| - |F_c||/\Sigma|F_o|$. $wR2 = \{\Sigma[w(F_o^2 - F_c^2)^2]/\Sigma[w(F_o^2)^2]\}^{1/2}$. [b] $GoF = [(\Sigma w|F_o| - |F_c|)^2/(N_{obs.} - N_{param.})]^{1/2}$.

essentially isolated with the shortest Y···Y distance being 8.211(2) Å. The Y···N (Y···O) distances in **IY** are in the range 2.495(2)–2.552(2) Å [2.452(2)–2.521(1) Å]. The Eu···N (Eu···O) distances are rather longer in **I**, being in the range 2.545(2)–2.951(2) Å [2.502(2)–2.546(2) Å]. There is a π···π interaction between the neighbouring phen ligands with a plane-to-plane distance of around 3.4–3.6 Å. There are only weak C–H···O interactions in **I**.

Compound **I-5c** is a mononuclear $Eu^{3+}$ complex coordinated by three chelating nitrate ions and two bidentate 5-chloro-1,10-phenanthroline ligands. The ligand is disordered such that Cl1 is disordered with Cl3, and Cl2 with Cl4. The coordination geometry is described as a distorted bicapped square antiprism (bottom square: O1/O2/O4/O5; top square: O8/N4/N5/N6 bicapped by O7 and N7; the dihedral angle between the top and bottom planes is 3.21°). One ligand has the phenanthroline plane (N4/N5/C1–C12) nearly parallel (3.51°) to that of the top square whereas the other ligand (N6/N7/C13–C24) is orthogonal (86.7°) to it. Only weak intra- and intermolecular C–H···O hydrogen-bonding is observed. Neighbouring phenanthroline rings exhibit π···π interactions (between N6/C13–C16/C24, with an interplanar distance of 3.357 Å, and between N4/C1–C4/C12, with an interplanar distance of 3.348 Å). The molecules are packed efficiently in the lattice so that there is no void volume. Molecules in the lattice are related by an inversion centre. The Eu···N (Eu···O) distances are in the range 2.577(5)–2.586(5) Å [2.464(8)–2.527(4) Å].

Compound **I-4m** co-crystallized with $CH_3CN{\cdot}2H_2O$ whereas **I-5m** contains no solvent of crystallization in the unit cell. For each of these complexes the central $Eu^{3+}$ centre is 10-coordinate and consists of three nitrato anions and two bidentate methyl-substituted 1,10-phenanthroline ligands. The two phenanthroline planes make dihedral angles of 65.77 and 81.92° in **I-4m** and **I-5m**, respectively. Only weak intermolecular C–H···O hydrogen-bonding is apparent in the two complexes (2.495–2.718 Å for **I-4m**, 2.527–2.712 Å for **I-5m**). It is also clear that neighbouring phenanthroline rings display π···π interactions (3.506 Å for **I-4m** and 3.534 Å for **I-5m**). The Eu···N (Eu···O) distances are in the range 2.545(9)–2.611(10) Å [2.466(8)–2.554(8) Å] for **I-4m** whereas the corresponding values are 2.540(6)–2.566(6) Å [2.483(5)–2.558(5) Å] for **I-5m**.

## IR and Raman Spectra

Frames (a) and (b) of Figure 2 show the FTIR and Raman spectra of the complexes. They are particularly complicated and the detailed assignment of **I** has been attempted by Tsaryuk et al.[22] with the bands at 708, ca. 740, 813, 1030, ca. 1300 and 1480–1500 cm$^{-1}$ attributed to the vibrations of the nitrate group. The first two of these are too weak to be observed in Figure 2 (a) and the others do not exhibit marked shifts in the series of complexes. Unlike the spectra in ref.[22], a band at 1385 cm$^{-1}$ is evident in Figure 2 (a) for the samples prepared as KBr discs, which has been attributed to the $\nu_3(D_{3h})$ mode of liberated $NO_3^-$. The most intense bands in the range 1400–1650 cm$^{-1}$ in the Raman spectra correspond to the stretching vibrations of the aromatic ν(C=C) and heterocyclic ring ν(C=N) modes.[22] Discussions of these bands in the FTIR spectra have been in-

  

cluded elsewhere.[22,23] The Raman spectra in Figure 2 (b) show the shifts of the bands in this region more clearly. The strongest feature in the Raman spectrum of the phen·$H_2O$ ligand is at 1407 $cm^{-1}$, which corresponds to coupled ring-stretching vibrations. This band moves to 1421 $cm^{-1}$ in **I** and the frequencies in the other four complexes (between 1396 and 1420 $cm^{-1}$) are not readily rationalized.

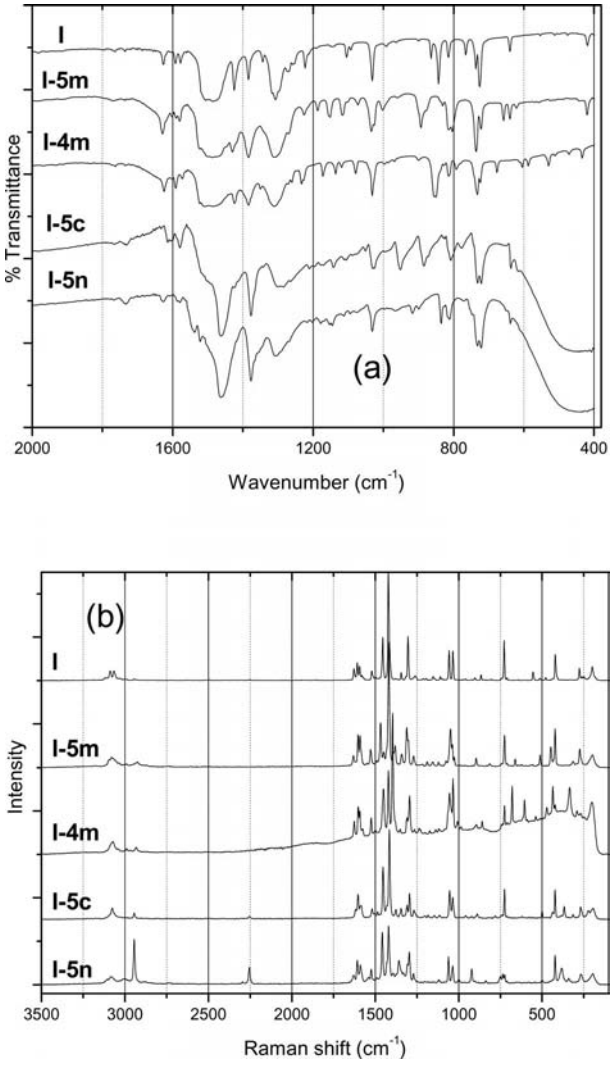


Figure 2. (a) FTIR spectra (400–2000 $cm^{-1}$) and (b) Raman spectra (100–3500 $cm^{-1}$) of europium complexes of phen derivatives. Nujol mulls were employed in (a) for **1**–**5c** and **1**–**5n** whereas KBr discs were employed for **I**, **I-5m** and **I-4m**.

The presence of a ν(CN) vibration at 2254 $cm^{-1}$ in Figure 2 (b) for the **I-5n** complex indicates the incorporation of MeCN solvent.

Tsaryuk et al.[22] assigned various bands between 143–275 $cm^{-1}$ in the far-IR spectrum of **I** to metal–ligand vibrations and noted that Eu–O modes are at 165 and 200 $cm^{-1}$ in the far-IR spectrum of $Eu(NO_3)_3·6H_2O$.

## UV Absorption Spectra

Substituents on the 1,10-phenanthroline molecule with different donor–acceptor properties can produce different effective charges on the nitrogen atoms and accordingly change the strength of the Eu–N bonds. This effect should be reflected in the absorption and excitation spectra of substituted phenanthroline complexes. The room-temperature UV absorption spectra of the substituted phenanthroline–europium complexes in MeCN solution are compared in Figure 3. All of the complexes show two strong bands corresponding to $\pi\rightarrow\pi^*$ transitions of the heterocyclic and aromatic rings with the maxima at 230 and 272 nm for **I**, 231 and 273 nm for **I-4m**, 233 and 276 nm for **I-5c**, 232 and 276 nm for **I-5m**, and 232 and 273 nm for **I-5n**. There is therefore a slight redshift of the absorption of the $\pi\rightarrow\pi^*$ transition that decreases in the order of **I-5m** > **I-5c** > **I-5n** > **I-4m** > **I**. There is a lower-energy shoulder evident in the spectra of Figure 3 (for example, at 293 nm for **I**), which corresponds to the $n\rightarrow\pi^*$ transition. This feature extends to much longer wavelengths for **I-5n**.

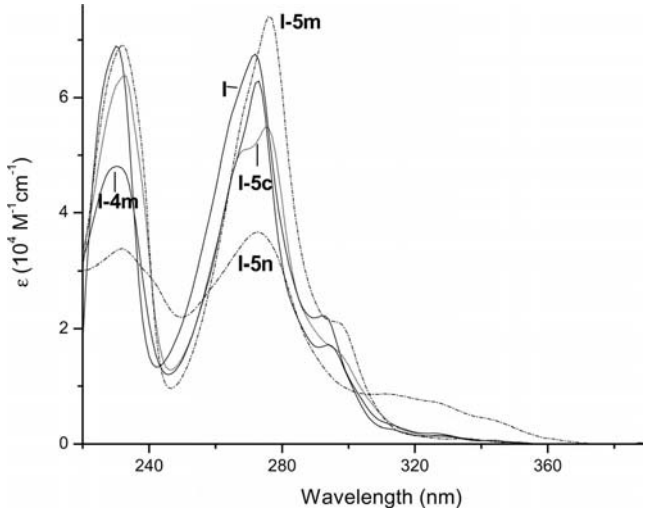


Figure 3. Room-temperature absorption spectra of europium complexes with substituted 1,10-phenananthroline derivatives in $CH_3CN$ solution.

## Excitation and Emission Spectra

Figure S5 shows the lowest-energy emission and excitation spectra of three of the phen derivatives and the luminescent electronic states are situated in the region of 28000–29000 $cm^{-1}$. These bands correspond to singlet-state emission. The room-temperature excitation spectra of the complexes derived by monitoring the emission of $Eu^{3+}$ at 615 nm are compared in Figure 4. The sharp absorption bands at longer wavelengths are typical of absorption by $Eu^{3+}$ from the $^7F_0$ ground state and the terminal multiplets are marked in the figure. The broad features at shorter wavelengths correspond to the antenna effect of phenanthroline and substituted phenanthroline ligands and indicate excitation transfer from the triplet state of these complexes. There is a gradual redshift from **I** to **I-5n**.

The room-temperature emission spectra of the phen and substituted phen complexes are compared in Figure 5. The emission spectra at room temperature exhibit typical fea-

  

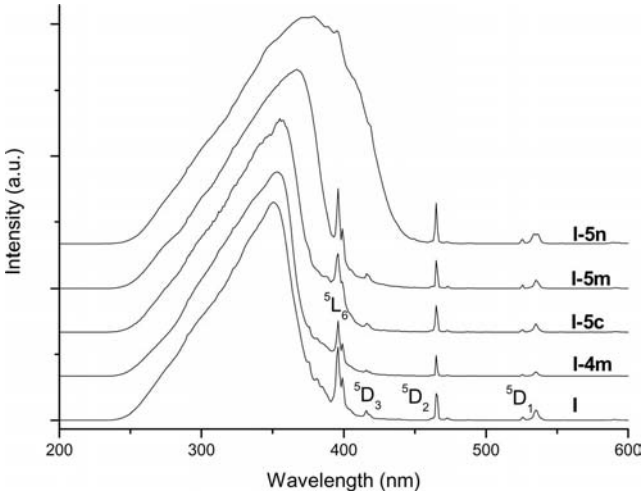


Figure 4. Room-temperature solid-state excitation spectra of europium complexes with substituted 1,10-phenananthroline derivatives obtained by monitoring the emission at 615 nm of $Eu^{3+}$. The initial state is $^7F_0$ and terminal $Eu^{3+}$ multiplets are marked. The relative intensities are arbitrary. The instrument sensitivity decreases rapidly at wavelengths less than 250 nm.

tures of $Eu^{3+}$ emission, dominated by the forced dipole transitions from $^5D_0$ to $^7F_J$ ($J$ = 0–4) with $\Delta J$ = 2, 4. The magnetic dipole transition $^5D_0 \rightarrow {}^7F_1$ is also prominent. The decay of emission from $^5D_0$ is monoexponential and the room-temperature lifetimes of the $^5D_0$ state of these complexes are similar, ranging from 0.985 to 1.071 ms (Table 2).

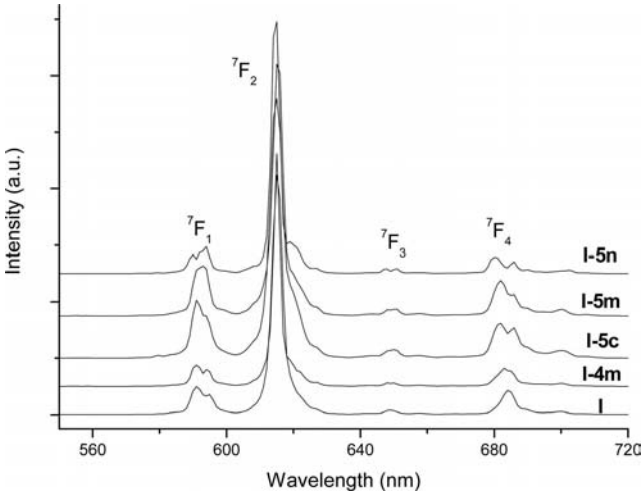


Figure 5. Room-temperature emission spectra of solid-state europium complexes with substituted 1,10-phenananthroline derivatives excited by 273 nm radiation. The luminescent state is $^5D_0$ and terminal multiplets are marked.

## Quantum Efficiency of Emission

The quantum efficiency of the luminescence from the complexes was determined by a comparative method in which the sample under examination in $CH_3CN$ solution was compared with a standard (quinine bisulfate in 0.1 M sulfuric acid solution) of known (error ±5%) quantum efficiency for excitation in the region 200–400 nm.[31] The measured values are compiled in Table 2 and fall in the range of 24 ± 3% except for **I-5n**. Similarly, the excitation spectra of the complexes in Figure 4, which show the donor ligand absorption bands, are at lower energy for **1**–**5n**. The lower quantum efficiency for **I-5n** is therefore associated with the unfavourable location of the ligand donor state relative to the $Eu^{3+}$ acceptor states such that back-transfer is enhanced relative to the scenarios of the other complexes.

Table 2. Quantum efficiencies[a] and lifetimes[b] of $^5D_0$ for the europium complexes.

| | Quantum efficiency [%] | Lifetime of $^5D_0$ [ms] |
|---|---|---|
| **I** | 21 | 0.995 |
| **I-5c** | 22 | 0.995 |
| **I-5m** | 26 | 1.071 |
| **I-4m** | 27 | 0.985 |
| **I-5n** | 9 | 0.996 |

[a] With an error of 15%. [b] With an error of 5%.

## High-Resolution Electronic Spectra

On cooling the complexes to 10 K, the emission bands sharpen so that fine structure due to individual crystal field transitions is observed. Spectral bands that arise from impurities or defect sites may be distinguished from $4f^6 \rightarrow 4f^6$ transitions in several ways. First, different excitation lines (465 and 355 nm) have been employed because the relative emission intensities of other features compared with $Eu^{3+}$ emission would be expected to change as the absorption characteristics differ. Secondly, the complexes were prepared by doping the corresponding $Y^{3+}$ complex with 0.5 at.-% $Eu^{3+}$. In this case the energy migration between $Eu^{3+}$, which often terminates at defect sites, is hindered. The 10 K emission spectra of neat and doped complexes are compared in Figure 6, in which transitions from $^5D_0$ to $^7F_J$ ($J$ = 1–4) multiplet terms are shown, with the transition to $^7F_2$ being most prominent. The spectral features in the neat and doped samples are similar, although more clearly resolved in the diluted samples, giving confidence to the quality of the data. The emission from $^5D_2$ is quenched by intramolecular non-radiative processes, whereas that from $^5D_1$ is very weak and not evident in the intensity scale used in Figure 6.

The emission transitions from $^5D_0$ to $^7F_J$ ($J$ = 0–4) of the complexes at 10 K are compared in more detail in Figure 7. Notably, the bands corresponding to the transition from $^5D_0$ to $^7F_{0-4}$ of **I** are much sharper than those of substituted phenanthroline–europium complexes, which is presumably due to disorder and inhomogeneous broadening in the latter cases. The very weak feature at highest energy (near 581 nm, between 17207–17216 $cm^{-1}$) corresponds to the $^5D_0 \rightarrow {}^7F_0$ transition. The forced dipole intensity of this transition occurs through $J$-mixing of $^7F_0$ (mainly with $^7F_2$) because the site symmetry of $Eu^{3+}$ is $C_2$ in **I** and $C_1$ in the other complexes. Three bands, corresponding to magnetic dipole transitions, are expected for the $^5D_0 \rightarrow {}^7F_1$ transition,

  

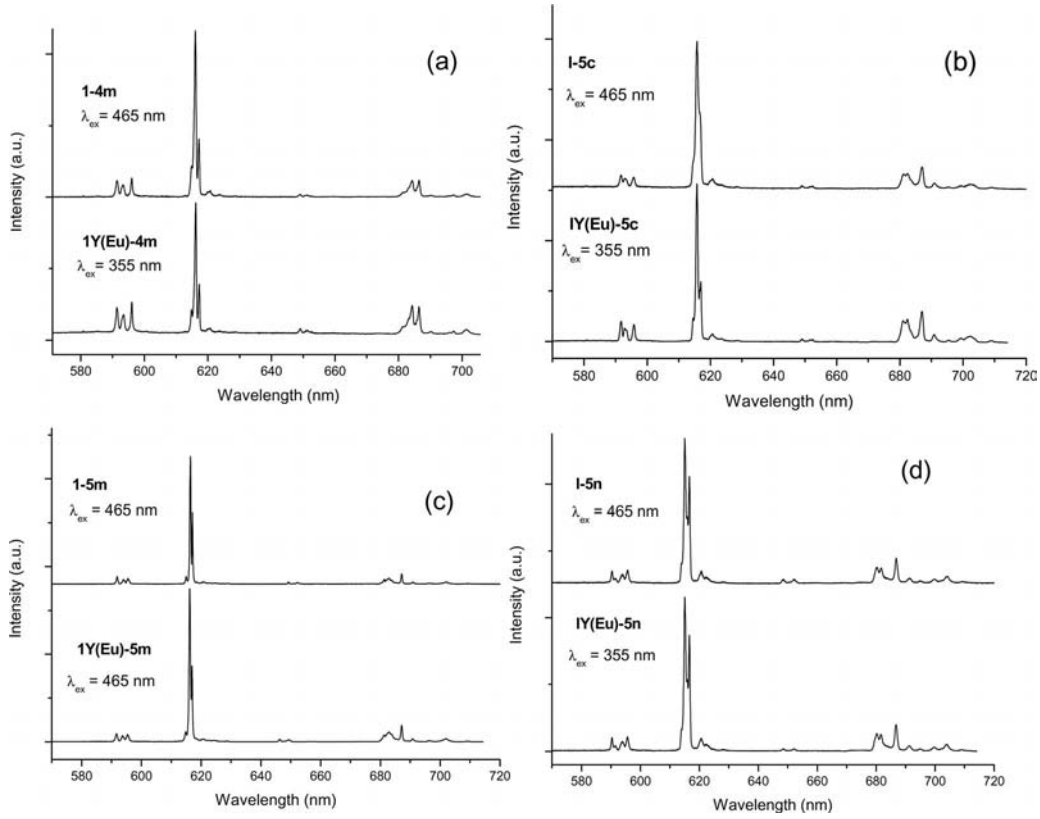


Figure 6. Comparison of 10 K luminescence spectra of neat and doped europium complexes of phen derivatives excited by radiation of 465 or 355 nm. The intensity scales are arbitrary.

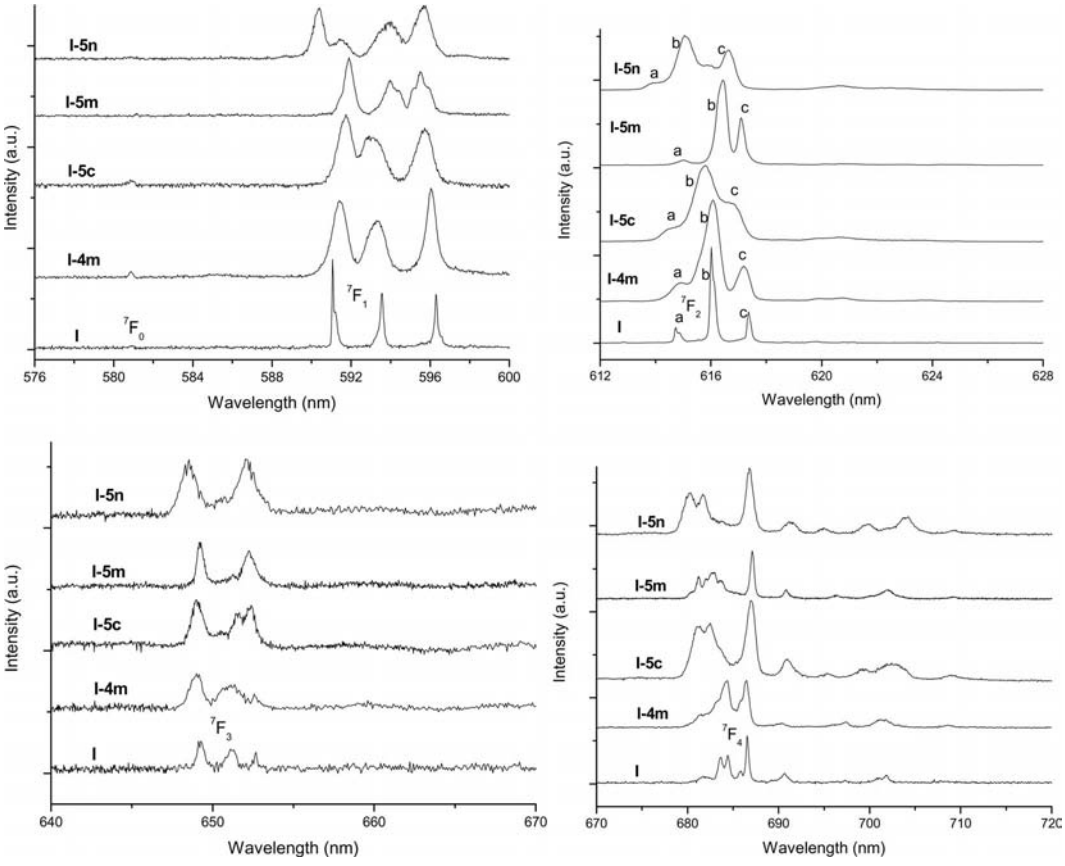


Figure 7. Luminescence spectra of europium complexes with phen and substituted phen ligands at 10 K excited by radiation of 465 nm.

  

but more are observed in all cases. The weaker structure is assigned to near-resonant phonon modes primarily involving $Eu^{3+}$ motions. Tsaryuk et al.[22] made a careful study of the vibronic sidebands of the $^7F_0 \rightarrow {}^5D_{0,2}$ transitions for several $Eu^{3+}$ complexes with substituted phen derivatives by metal replacement and ligand deuteriation so we have not pursued this topic further. Note, however, that the general structure of each complex for a particular $^5D_0 \rightarrow {}^7F_{1-4}$ transition is reasonably similar, although the band positions differ. For example, for $^5D_0 \rightarrow {}^7F_2$ in Figure 7 the highest-energy band is a weak feature (labelled a), then there is a strong band (b) and the lowest-energy band is of medium intensity (c). The first two of these bands are split in the more clearly resolved spectrum of **I**. Analyses of the spectra enabled the $^5D_0$ and $^7F_{0,1}$ energy levels to be determined for all systems, including the 5-amino-1,10-phenanthroline complex (**I-5a**, not shown), and a more complete energy level dataset to be constructed from the clearly resolved spectrum of **I** (Table 3, $E_{exp.}$).

Table 3. Energy levels [$cm^{-1}$] and crystal field fitting for **I**.[a]

| Level # | $^{2S+1}L_J$ | IR | $E_{exp.}$ | $E_{full}$ | $\Delta E_1$ | $E_{s/w}$ | $\Delta E_2$ |
|---|---|---|---|---|---|---|---|
| 1 | $^7F_0$ | 1 | 0 | 9 | –9 | 10 | –10 |
| 2 | $^7F_1$ | 1 | 295 | 293 | 2 | 302 | –7 |
| 3 | $^7F_1$ | 2 | 367 | 374 | –7 | 374 | –7 |
| 4 | $^7F_1$ | 2 | 444 | 459 | –15 | 451 | –7 |
| 5 | $^7F_2$ | 2 | 947 | 941 | 6 | 946 | 2 |
| 6 | $^7F_2$ | 2 | 981 | 970 | 11 | 970 | 11 |
| 7 | $^7F_2$ | 1 | 1016 | 1009 | 7 | 1014 | 2 |
| 8 | $^7F_2$ | 1 | 1080 | 1050 | 30 | 1045 | 35 |
| 9 | $^7F_2$ | 1 | 1111 | 1097 | 14 | 1091 | 20 |
| 10 | $^7F_3$ | 2 | | 1749 | | 1753 | |
| 11 | $^7F_3$ | 1 | | 1771 | | 1770 | |
| 12 | $^7F_3$ | 2 | 1808 | 1811 | –3 | 1811 | –3 |
| 13 | $^7F_3$ | 1 | 1846 | 1833 | 13 | 1831 | 16 |
| 14 | $^7F_3$ | 2 | 1857 | 1860 | –3 | 1858 | –1 |
| 15 | $^7F_3$ | 2 | 1893 | 1893 | 0 | 1893 | 0 |
| 16 | $^7F_3$ | 1 | | 1896 | | 1895 | |
| 17 | $^7F_4$ | 2 | 2587 | 2581 | 7 | 2582 | 5 |
| 18 | $^7F_4$ | 1 | 2603 | 2616 | –13 | 2617 | –14 |
| 19 | $^7F_4$ | 1 | 2633 | 2626 | 7 | 2626 | 7 |
| 20 | $^7F_4$ | 2 | 2648 | 2674 | –26 | 2675 | –27 |
| 21 | $^7F_4$ | 1 | 2735 | 2737 | –2 | 2736 | –1 |
| 22 | $^7F_4$ | 1 | 2872 | 2879 | –7 | 2879 | –7 |
| 23 | $^7F_4$ | 1 | 2946 | 2957 | –11 | 2956 | –10 |
| 24 | $^7F_4$ | 2 | 2967 | 2967 | 0 | 2969 | –2 |
| 25 | $^7F_4$ | 2 | 3086 | 3086 | 0 | 3085 | 2 |
| 50 | $^5D(3)_0$ | 1 | 17241 | 17263 | –22 | 17262 | –21 |
| 51 | $^5D(3)_1$ | 1 | 18945 | 18922 | 23 | 18924 | 22 |

[a] IR irreducible representation in $C_2$; $E_{exp.}$ is the experimentally determined energy, $E_{s/w}$ and $E_{full}$ are the two energy level fits (stepwise and full), as described in the text with the corresponding energy deviations from experiment of $\Delta E_1$ and $\Delta E_2$.

## Crystal Field Calculations

The primary aim of this study was to find the relationship between derived parameters from the spectra of the $Eu^{3+}$ complexes and other physical quantities. To accomplish this, crystal field calculations were performed to the maximum possible extent. The site symmetry of $Eu^{3+}$ in these complexes is at most $C_2$ so that too many parameters are required to perform a full crystal field calculation. We therefore followed the conventional procedure by approximating the site symmetry as $C_{2v}$, which is equivalent to $D_{2h}$ for the even part of the crystal field interactions involved in energy level calculations. The usual semi-empirical hamiltonian for $4f^N$ electrons was employed in the calculations.[32]

The spin–orbit coupling parameter $\zeta_{4f}$ and second-rank crystal-field parameters $B_0^2$ and $B_2^2$ were obtained from the three energy differences between the four energy levels of $^7F_0$ and $^7F_1$. There are six equivalent choices of $B_0^2$ and $B_2^2$, which are linked by six different but equivalent choices of $z$ axis in the $D_2$ symmetry. The link between each of the six choices of the set of $B_0^2$ and $B_2^2$ and the particular choice of the $z$ axis for $Eu^{3+}$ in the complex is not likely to be made in a known way, since $B_0^2$ and $B_2^2$ are not short-range parameters. Thus, for a given choice of $z$ axis fixed to the ligand arrangements, it is not known which set of parameters should be used. One choice of parameters for the set of complexes is listed in Table 4, with the rationale and the complete sets for **I** listed in Table S8 (see Supporting Information). Table 4 also presents, in the last column, the second-rank crystal field strength, $s_2$, of the complexes. Although the crystal field strength is greatest for the $NO_2$-substituted phen complex, with the largest Taft $\sigma^*$ constant (Table S11), there is no clear relationship between the second-rank crystal field strengths of the other complexes and Taft constants. In particular, there is a large difference in these crystal field strengths for $Eu^{3+}$ in **I** and **IY**, with the mean metal–oxygen bond length 1.7% shorter for the latter.

Table 4. Energy parameters obtained from the emission energies of the $^5D_0 \rightarrow {}^7F_{0,1}$ transitions for the seven complexes. All values are in $cm^{-1}$.

| | $F^2$ | $\zeta_{4f}$ | $B_0^2$ | $B_2^2$ | $s_2$[a] |
|---|---|---|---|---|---|
| **I** | 70298 | 1321 | –380 | –158 | 197 |
| **IY** | 70212 | 1317 | –279 | –95 | 138 |
| **I-5n** | 70277 | 1305 | –441 | –103 | 208 |
| **I-5m** | 70177 | 1319 | –277 | –89 | 136 |
| **I-4m** | 70181 | 1322 | –317 | –161 | 175 |
| **I-5a** | 70182 | 1324 | –259 | –164 | 155 |
| **I-5c** | 70216 | 1318 | –257 | –162 | 154 |

[a] The $k^{th}$-order crystal field strength $s_k$ of the crystal field parameters is defined by $s_k^2 = (2k+1)^{-1}\left[(B_0^k)^2 + 2\sum_{q=0}^{k} |B_q^k|^2\right]$.

A more comprehensive calculation was performed on **I** by making certain assumptions. To determine the fourth-rank crystal field parameters, the choice of Puntus and Zolin[25] was followed by assuming $B_0^4$ to be negative with the largest absolute value. To determine the sixth-rank crystal field parameters, the $B_q^2$ and $B_q^4$ parameters were fixed and fittings were attempted by assuming that one of the $B_q^6$ ($q$ = 0, 2, 4, 6) parameters dominates with the possibility that it is positive or negative. It turns out that the fit that treated $B_2^6$ as negative and as the most important sixth-rank parameter gave the best fitting among all the choices. The parameters obtained were further optimized by either constrain-

  

ing $B_q^2$ to give the exact $^7F_1$ splitting (stepwise fit, s/w) or optimizing all $B_q^k$ together for all the measured levels together (full optimization fit, full). The $F^2$, $\zeta_{4f}$, $B_0^2$ and $B_2^2$ parameters were calculated from the energies of the emissions of $^5D_0$ to $^7F_{0,1}$. The parameters $F^2$ and $\zeta_{4f}$ are quasi-free ion parameters that may change as a result of the covalency between the free ion and nearest-neighbour ligands. The values corresponding to set 3 of Table S8 for **I** using full or stepwise calculations are given in Table S10. The $B_0^2$ and $B_2^2$ parameters may contain substantial contributions from long-distance surrounding atoms and hence change drastically. The average deviation of calculated to measured energy levels does not improve by allowing $B_q^2$ to vary along with $B_q^4$ and $B_q^6$.

The predicted energy levels are listed for the two fittings ($E_{full}$, $E_{s/w}$) for comparison with the experimental data in Table 3 and a more complete listing is given in Table S9. Note that if the signs of $B_2^k$ ($k$ = 2, 4, 6) and $B_6^6$ are simultaneously changed, the predicted energy levels will be exactly the same because such a change corresponds to a rotation of 90° around the nominal $z$ axis used.

## Conclusions

The crystal structures and optical spectroscopic data of selected europium complexes with substituted 1,10-phenanthroline derivatives have been presented in this report. Although the 10-coordinate geometries of all the complexes are similar, comprising three chelating nitrato anions and two bidentate phen derivatives, the crystal structures fall into three different space groups (Table 1). The room-temperature emission spectra for all the complexes (Figure 5) are dominated by the forced electric dipole transition $^5D_0 \rightarrow {}^7F_2$. This is compatible with the absence of an inversion centre for $Eu^{3+}$. The purity of the complexes was checked not only by comparison with the corresponding $Y^{3+}$ complexes doped with $Eu^{3+}$ but also by comparison of the emission spectra using different laser excitation lines (Figure 6). The quantum efficiencies are moderate (Table 2) with the exception of the nitro-substituted phen derivative **I-5n**. The poor quantum efficiency of this complex has been attributed to the rather low energy of the ligand donor state, as shown in the excitation spectra (Figure 4). The ligand–metal transfer efficiency depends partly upon the relative location of the donor–acceptor electronic energy levels. The complexes have a good ligand emission spectral overlap with the $Eu^{3+}$ $^7F_0 \rightarrow {}^5D_2$ acceptor transition, except for **I-5n**, for which the metal–ligand back-transfer is faster. The acceptor transition is forced electric dipole allowed. Ligand–metal transfer involving the $^5D_1$ $Eu^{3+}$ acceptor state is unlikely because the $^7F_0 \rightarrow {}^5D_1$ transition is magnetic dipole in character so that the electronic matrix element for transfer probability is much smaller. Malta[33,34] has provided selection rules for multi-polar and exchange mechanisms of ligand–metal transfer and transfer to $^5D_1$ is only allowed by the latter mechanism. These considerations of the poorer quantum yield of emission of **I-5n** compared with, for example, **I**, resulting from poorer ligand–metal transfer, are shown diagrammatically in Figure 8. A reviewer has pointed out a further mechanism to account for the lower quantum efficiency of **I-5n** by citing the efficient electron-transfer mechanisms that nitro compounds are well-known to provide in the quenching of luminescence. Note that the $Eu^{3+}$ luminescence lifetime, which reflects the importance of intra- and interionic processes upon the $^5D_0$ state, is similar for all the complexes studied.

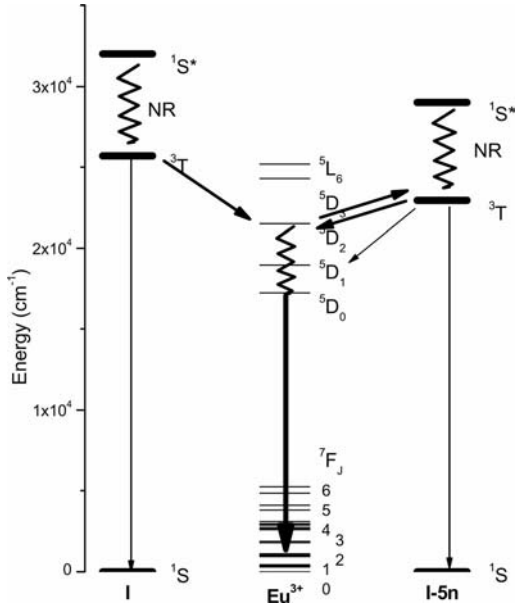


Figure 8. Schematic diagram of the ligand–metal energy transfer for **I** and **I-5n**.

The electronic emission spectrum of **I** is more clearly resolved than for the other complexes. The band-broadening is attributed to disorder in the latter complexes, as shown explicitly in the crystal structure of **I-5c**. A detailed crystal field analysis could therefore be performed for **I**, whereas only a comparison of $^7F_1$ energy levels was feasible for the other complexes. The energy level fit for **I** using a pseudo-symmetry that requires few parameters gives reasonable results (Tables 3 and S9). No simple correlations or relationships were found for the luminescence band positions, derived $^7F_1$ energy levels or second-rank crystal field strengths versus the Taft constants or crystallographic data. The spectral band positions not only depend upon the metal–ligand coordination geometry, but also upon the detailed crystal structure and site symmetry of $Eu^{3+}$. Also, the second-rank crystal field parameters are a long-range probe of the metal ion environment and thus simple relations with metal–ligand bond lengths or angles may not be anticipated.

## Experimental Section

**Reagents:** All substituted 5(or 4)-R-1,10-phenanthroline ligands (R = chloro, methyl, nitro, amino) (Aldrich, analytical grade) were used as received without further purification. $Eu_2O_3$ (99.99%) was purchased from International Laboratory. $Eu(NO_3)_3{\cdot}xH_2O$ was ob-

  

tained by dissolving $Eu_2O_3$ in dilute aqueous nitric acid followed by slow evaporation.

**Synthesis of I-5c:** A solution of 5-chloro-1,10-phenanthroline (85.9 mg, 0.4 mmol) in MeCN (10 mL) was added to a solution of $Eu(NO_3)_3$ (67.6 mg, 0.2 mmol) in MeCN (5 mL). The mixture was left undisturbed for 1 week; white needle-shaped crystals were obtained. $C_{24}H_{14}Cl_2EuN_7O_9$ (767.28): calcd. C 37.57, H 1.84, N 12.78; found C 37.57, H 1.929, N 12.69.

**Synthesis of I-5m:** A solution of 5-methyl-1,10-phenanthroline (77.7 mg, 0.4 mmol) in MeCN (10 mL) was added to a solution of $Eu(NO_3)_3$ (67.6 mg, 0.2 mmol) in MeCN (10 mL). The mixture was left undisturbed for 1 week; white block-shaped crystals were obtained. $C_{26}H_{20}EuN_7O_9$ (726.44): calcd. C 42.99, H 2.78, N 13.50; found C 42.88, H 2.879, N 13.41.

**Synthesis of I-4m:** A solution of 4-methyl-1,10-phenanthroline (77.7 mg, 0.4 mmol) in MeCN (10 mL) was added to a solution of $Eu(NO_3)_3$ (67.6 mg, 0.2 mmol) in MeCN (10 mL). The mixture was left undisturbed for 2 weeks; white block-shaped crystals were obtained. $C_{28}H_{27}EuN_8O_{11}$ (803.52): calcd. C 41.85, H 3.39, N 13.95; found for separate preparations H 3.04/3.04, N 12.0/14.8. We were unable to obtain a reliable carbon analysis, which has been attributed to the presence of solvent molecules.

**Synthesis of I-5n:** A solution of 5-nitro-1,10-phenanthroline (90.1 mg, 0.4 mmol) in MeCN (10 mL) was added to a solution of $Eu(NO_3)_3$ (67.6 mg, 0.2 mmol) in MeCN (10 mL). The mixture was left undisturbed for 1 week; white block-shaped crystals were obtained. $C_{24}H_{14}N_9O_9Eu$ (724.39): calcd. C 36.56, H 1.79, N 15.99; found C 36.86, H 2.125, N 16.41.

**Diluted Crystals:** The diluted systems **IY(Eu)** were analogously prepared from mixed $Y_{0.995}Eu_{0.005}(NO_3)_3$ solutions. The above complexes were also synthesized by a solvothermal method by placing the solutions in a Teflon®-lined stainless steel autoclave and heating in an oven at 120 °C for 15 h. The precipitate was filtered, washed with ethanol and dried at 80 °C for 12 h.

**X-ray Crystallography:** The crystal structures were determined at The University of Hong Kong [**I**, **IY**, **IY(Eu)** and **I-5c**] and at Hong Kong Baptist University (**I-4m** and **I-5m**). X-ray diffraction data were collected at 293 K using graphite-monochromated Mo-$K_\alpha$ radiation ($\lambda$ = 0.71073 Å) with a Bruker AXS SMART 1000 CCD diffractometer. The collected frames were processed with the SAINT+ [35] software and an absorption correction (SADABS)[36] was applied to the collected reflections. The structure was solved by the direct or Patterson methods (SHELXTL)[37] in conjunction with standard difference Fourier techniques and subsequently refined by full-matrix least-squares analyses on $F^2$. Hydrogen atoms were generated in their idealized positions and all non-hydrogen atoms were refined anisotropically. Crystal parameters and results of structure refinements are given in Table 2.

CCDC-778298 (for **I**), -778296 (for **IY**), -778295 [for **IY(Eu)**], -778297 (for **I-5c**), -778299 (for **I-4m**) and -778300 (for **I-5m**) contain the supplementary crystallographic data for this paper. These data can be obtained free of charge from The Cambridge Crystallographic Data Centre via www.ccdc.cam.ac.uk/data_request/cif.

**Photophysical Measurements:** The FTIR absorption spectra of all the samples as either KBr discs or Nujol mulls were recorded between 200–4000 $cm^{-1}$ at a resolution of 2–4 $cm^{-1}$ at room temperature using a Bomem MB-120 spectrometer. Complexes **I-5c** and **I-5n** undergo decomposition when in contact with KBr so these two samples were ground with Nujol to make a thin mull between NaCl plates. The UV/Vis absorption spectra of the complexes in MeCN solutions were measured with an Agilent 8453 spectrophotometer. The emission and excitation spectra were measured with a Horiba Jobin Yvon Fluorolog spectrofluorimeter using a xenon lamp as the light source and the signal was detected using a Hamamatsu R636 photomultiplier. The absorption and emission spectra were used to calculate the quantum efficiency of each sample by using Equation (1)[38] in which $n$ is the refractive index of the solvent, $D$ is the integrated intensity of the emission spectrum and $B$ is the fraction of light absorbed by the sample at the excitation wavelength, which is determined by Equation (2), in which $A$ is the absorbance [$cm^{-1}$] and $L$ [cm] is the optical path length. 0.1 M $H_2SO_4$ solution of quinine sulfate (f = 0.546) was used as the reference.

$$\phi_s = \phi_r\left(\frac{B_r}{B_s}\right)\left(\frac{n_s}{n_r}\right)^2\left(\frac{D_s}{D_r}\right) \quad (1)$$

$$B = 1–10^{-AL} \quad (2)$$

The luminescence lifetime was also analyzed with a 0.25 m Jobin–Yvon monochromater using a flash lamp as the pumping source. The signal was detected by a Hamamatsu R636 photomultiplier with a TBX-04-A single-photon detection module. Emission spectra with a resolution of 2–4 $cm^{-1}$ were recorded using an air-cooled Omnichrome $Ar^+$ laser or a Panther optical parametric oscillator (OPO) system pumped by the second harmonic of a Surelite $Nd^{3+}$:YAG laser. The samples were mounted in an Oxford Instruments closed-cycle cryostat with base temperature of 10 K. The emissions were collected through a 0.5 m Acton spectrometer equipped with a SpectruMM CCD detector.

**Supporting Information** (see footnote on the first page of this article): Schematic molecular structures; Ortep plot and packing diagrams of **IY**; bond lengths; UV absorption, excitation and emission spectra of phen derivatives; 10 K emission spectra of **IY(Eu)**; energies of $^5D_0 \rightarrow {}^7F_0$ transition, derived $^7F_1$ levels, and vibronic structures of $^5D_0 \rightarrow {}^7F_1$ for the $Eu^{3+}$ complexes; equivalent sets of $B_0^2$ and $B_2^2$ parameters for the $Eu^{3+}$ in complex **I**; predicted energy levels of **I**; fully optimized and stepwise parameter sets for the fitting of the $Eu^{3+}$ energy levels in **I**; Taft sigma constants.

## Acknowledgments

P. A. T. acknowledges financial support for this project from the Hong Kong University Grants Council Research (Grant City, U 102607). This work was also supported by the National Natural Science Foundation of China (grant number 10804099). We are grateful to Prof. M. Hasegawa for sending reprints of his publications.

[1] L. Ozawa, M. Itoh, *Chem. Rev.* **2003**, *103*, 3835–3855.
[2] R. C. Evans, P. Douglas, C. J. Winscom, *Coord. Chem. Rev.* **2006**, *250*, 2093–2126.
[3] S. Capecchi, O. Renault, D. G. Moon, M. Halim, M. Etchells, P. J. Dobson, O. V. Salata, V. Chrisou, *Adv. Mater.* **2000**, *12*, 1591–1594.
[4] H. Xin, F. Y. Li, M. Shi, Z. Q. Bian, C. H. Huang, *J. Am. Chem. Soc.* **2003**, *125*, 7166–7167.
[5] J. F. Wang, R. Y. Wang, J. Yang, Z. P. Zheng, M. Carducci, T. Cayou, N. Peyghambarian, G. E. Jabbour, *J. Am. Chem. Soc.* **2001**, *123*, 6179–6180.
[6] G. H. Jia, G.-L. Law, K.-L. Wong, P. A. Tanner, W.-T. Wong, *Inorg. Chem.* **2008**, *47*, 9431–9438.
[7] G.-L. Law, K.-L. Wong, Y.-Y. Yang, Q.-Y. Yi, G. H. Jia, W.-T. Wong, P. A. Tanner, *Inorg. Chem.* **2007**, *46*, 9754–9759.

  

[8] J. Kido, Y. Okamoto, *Chem. Rev.* **2002**, *102*, 2357–2368.
[9] G. A. Hebbink, D. N. Reinhoudt, F. C. J. M. van Veggel, *Eur. J. Org. Chem.* **2001**, *21*, 4101–4206.
[10] L. J. Martin, M. J. Hähnke, M. Nitz, J. Wöhnert, N. R. Silvaggi, K. N. Allen, H. Schwalbe, B. Imperiali, *J. Am. Chem. Soc.* **2007**, *129*, 7106–7113.
[11] J. C.-G. Bünzli, *Chem. Rev.* **2010**, *110*, 2729–2755.
[12] N. Sabbatini, M. Guardigli, I. Manet, *Handbook on the Physics and Chemistry of Rare Earths*, vol. 23 (Eds.: K. A. Gschneidner Jr., L. Eyring), North-Holland, Amsterdam, **1996**, p. 69–119.
[13] Y. Wan, L. Zhang, L. Lin, S. Gao, S. Lu, *Inorg. Chem.* **2003**, *42*, 4985–4994.
[14] P. Lenaerts, C. Görller-Walrand, K. Binnemans, *J. Lumin.* **2006**, *117*, 163–169.
[15] M. Flores, U. Caldino, R. Arroyo, *Opt. Mater.* **2006**, *28*, 514–518.
[16] L. Armelao, S. Quici, F. Barigelletti, G. Accorsi, G. Bottaro, M. Cavazzini, E. Tondello, *Coord. Chem. Rev.* **2010**, *254*, 487–505.
[17] J. Ritchie, A. Ruseckas, P. André, C. Münther, M. Van Ryssen, D. E. Vize, J. A. Crayston, I. D. W. Samuel, *Synth. Met.* **2009**, *159*, 583–588.
[18] M. Fernandes, V. de Zea Bermudez, R. A. Sá Ferreira, L. D. Carlos, A. Charas, J. Morgado, M. M. Silva, M. J. Smith, *Chem. Mater.* **2007**, *19*, 3892–3901.
[19] M. Hasegawa, *J. Photochem. Photobiol. A: Chem.* **2006**, *178*, 220–224.
[20] A. G. Mirochnik, B. V. Bukvetskii, P. A. Zhikhareva, V. E. Karasev, *Russ. J. Coord. Chem.* **2001**, *27*, 443–448.
[21] A. Boudalis, V. Nastopoulos, S. P. Perlepes, *Trans. Met. Chem.* **2001**, *26*, 276–281.
[22] V. Tsaryuk, V. Zolin, L. Puntus, V. Savchenko, J. Legendziewicz, J. Sokolnicki, R. Szostak, *J. Alloys Compd.* **2000**, *300–301*, 184–192.
[23] V. Tsaryuk, V. Zolin, J. Legendziewicz, *Spectrochim. Acta A* **1998**, *54*, 2247–2254.
[24] V. Tsaryuk, J. Legendziewicz, L. Puntus, V. Zolin, J. Sokolnicki, *J. Alloys Compd.* **2000**, *300–301*, 464–470.
[25] L. N. Puntus, V. Zolin, *Russ. J. Coord. Chem.* **2003**, *29*, 574–581.
[26] V. Tsaryuk, V. Zolin, J. Legendziewicz, R. Szostak, J. Sokolnicki, *Spectrochim. Acta A* **2005**, *61*, 185–191.
[27] V. Tsaryuk, V. Zolin, J. Legendziewicz, J. Sokolnicki, R. Szostak, *J. Lumin.* **2003**, *102–103*, 744–750.
[28] L. N. Puntus, K. A. Lyssenko, M. Y. Antipin, J. C.-G. Bünzli, *Inorg. Chem.* **2008**, *47*, 11095–11107.
[29] L. N. Puntus, K. P. Zhuravlev, I. S. Pekareva, K. A. Lyssenko, V. F. Zolin, *Opt. Mater.* **2008**, *30*, 806–809.
[30] L. Puntus, K. Lyssenko, *J. Rare Earths* **2008**, *26*, 146–152.
[31] M. S. Wrighton, D. S. Sinley, D. L. Morse, *J. Phys. Chem.* **1974**, *78*, 2229–2233.
[32] C. Görller-Walrand, K. Binnemans, *Handbook on the Physics and Chemistry of Rare Earths*, vol. 23 (Eds.: K. A. Gschneidner Jr., L. Eyring) North-Holland, Amsterdam, The Netherlands, **1996**, p. 121–283.
[33] O. L. Malta, *J. Lumin.* **1997**, *71*, 229–236.
[34] O. L. Malta, F. R. Goncalves e Silva, *Spectrochim. Acta* **1998**, *54*, 1593–1599.
[35] *SAINT*+, ver. 6.02a, Bruker Analytical X-ray System, Inc., Madison, WI, USA, **1998**.
[36] G. M. Sheldrick, *SADABS, Empirical Absorption Correction Program*, University of Göttingen, Göttingen, Germany, **1997**.
[37] G. M. Sheldrick, *SHELXTLTM*, reference manual, ver. 5.1, Madison, WI, USA, **1997**.
[38] J. N. Demas, G. A. Crosby, *J. Phys. Chem.* **1971**, *75*, 991–1024.

Received: August 25, 2010
Published Online: January 10, 2011

  